

High-*Z* benchmarking: Probing the sub-eV frontier and an extensive Li-like uranium atomic dataset

Shuang Li(李双), Yan Wang(王燕), Xue-Lian Chong(崇雪莲), Yan-Ran Luo(罗嫣然), and Fan Zhang(张凡)
Citation: Chin. Phys. B, 2026, 35 (**2**): 023103. DOI: 10.1088/1674-1056/ae311a
http://cpb.iphy.ac.cn; http://iopscience.iop.org/cpb

What follows is a list of articles you may be interested in

Benchmarking calculations of excitation energies and transition properties with spectroscopic accuracy of highly charged ions used for the fusion plasma and astrophysical plasma

Chunyu Zhang(张春雨), Kai Wang(王凯), Ran Si(司然), Jinqing Li(李金晴), Changxian Song(宋昌仙), Sijie Wu(吴思捷), Bishuang Yan(严碧霜), and Chongyang Chen(陈重阳)
Chin. Phys. B, 2023, 32 (**11**): 113102. DOI: 10.1088/1674-1056/acef07

Dynamic polarizabilities of the clock states of Al^+

Yuan-Fei Wei(魏远飞), Zhi-Ming Tang(唐志明), Cheng-Bin Li(李承斌), Yang Yang(杨洋), Ya-Ming Zou(邹亚明), Kai-Feng Cui(崔凯枫), and Xue-Ren Huang(黄学人)
Chin. Phys. B, 2022, 31 (**8**): 083102. DOI: 10.1088/1674-1056/ac5880

Calculations of atomic polarizability for beryllium using MCDHF method

Hui Dong(董辉), Jun Jiang(蒋军), Zhongwen Wu(武中文), Chenzhong Dong(董晨钟), and Gediminas Gaigalas
Chin. Phys. B, 2021, 30 (**4**): 043103. DOI: 10.1088/1674-1056/abd92d

Theoretical study of the hyperfine interaction constants, Landé *g*-factors, and electric quadrupole moments for the low-lying states of the $^{61}Ni^{q+}$ (q=11, 12, 14 , and 15) ions

Ting-Xian Zhang(张婷贤), Yong-Hui Zhang(张永慧), Cheng-Bin Li(李承斌), and Ting-Yun Shi(史庭云)
Chin. Phys. B, 2021, 30 (**1**): 013101. DOI: 10.1088/1674-1056/abc7a3

Forbidden transition properties of fine-structure $2p^3\,{}^4S_{3/2}$-$2p^3\,{}^2D_{3/2,5/2}$ for nitrogen-like ions

Xiao-Kang He(何晓康), Jian-Peng Liu(刘建鹏), Xiang Zhang(张祥), Yong Shen(沈咏), Hong-Xin Zou(邹宏新)
Chin. Phys. B, 2018, 27 (**8**): 083102. DOI: 10.1088/1674-1056/27/8/083102

DATA PAPER

High-Z benchmarking: Probing the sub-eV frontier and an extensive Li-like uranium atomic dataset

Shuang Li(李双)†, Yan Wang(王燕), Xue-Lian Chong(崇雪莲), Yan-Ran Luo(罗嫣然), and Fan Zhang(张凡)

School of Electrical and Optoelectronic Engineering, West Anhui University, Luan 237012, *China*

(Received 21 October 2025; revised manuscript received 19 December 2025; accepted manuscript online 25 December 2025)

Recent theoretical investigations into the excitation energies of the high-Z lithium isoelectronic sequence (Li-like) ions have revealed significant discrepancies [*Eur. Phys. J. Plus* **137** 1253 (2022)], with deviations between the methods employed reaching up to ~ 40 eV for U^{89+}. In this work, we address this issue through a comprehensive study of Li-like uranium (U^{89+}), calculating the lowest 35 levels of the $1s^2nl$ ($n \leq 6$) configurations. We employ two independent relativistic methods: the multiconfiguration Dirac–Hartree–Fock (MCDHF) method implemented in the GRASP2K code, and the relativistic configuration interaction (RCI) method within the Flexible Atomic Code (FAC). Our calculations resolve the discrepancies, achieving excellent mutual agreement and reducing deviations from experimental benchmarks to within ~ 2 eV. Furthermore, we identify the bottlenecks to achieving sub-eV accuracy for each method in the strong-field, high-Z regime. To the best of our knowledge, this is the most extensive dataset for this ion to date, including excitation energies, lifetimes, and radiative properties for allowed (E1) and forbidden (M1, E2, M2) transitions. Estimated uncertainties for most strong allowed and forbidden transitions remain below 1% and 2%, respectively, rendering this dataset valuable for applications in plasma spectroscopy. The dataset that supported the findings of this study is available in Science Data Bank at https://doi.org/10.57760/sciencedb.32492.

Keywords: multiconfiguration Dirac–Hartree–Fock, relativistic configuration interaction, quantum electrodynamics

PACS: 31.15.ag, 31.15.am, 31.15.xr, 32.70.Cs

DOI: 10.1088/1674-1056/ae311a **CSTR:** 32038.14.CPB.ae311a

1. Introduction

The rapid neutron-capture process (r-process) associated with compact object mergers,[1] particularly binary neutron star coalescence, produces substantial quantities of heavy actinides, including uranium. As the opacity of the resulting kilonova radiation is governed significantly by these heavy elements, the theoretical interpretation of such spectra demands a rigorous treatment of strong-field quantum electrodynamics (QED) effects[2–4] in the high-Z (high nuclear charge) regime. The high-Z lithium-like isoelectronic sequence (Li-like ions)[5,6] offers an ideal platform for validating QED effects and the Breit contributions,[7] owing to the substantial suppression of electron correlation in these systems. Within general-purpose atomic structure codes, QED contributions are typically confined to leading-order corrections, specifically self-energy (SE) and vacuum polarization (VP).[8–10] Consequently, a rigorous assessment of the Breit interaction and QED effects in the atomic codes is a prerequisite for the advancement of theoretical kilonova models. Moreover, accurate atomic parameters for high-Z Li-like ions are of significant value for x-ray laser research[11] and plasma spectroscopy calibration.[12]

In the mid-Z regime, using two independent relativistic methods, i.e., MCDHF (using the GRASP2K 2018 release[13,14]) and RCI (using FAC[15]), we have previously achieved sub-eV precision for Li-like ions, such as Fe^{23+} [5] and Ge^{29+},[6] confirming the robustness and mutual consistency of these frameworks.

However, whether this consistency persists in the high-Z limit remains an open question. Recent work,[16] providing a comprehensive dataset for Li-like ions ($Z = 57$–92), brings this issue into focus. Although the authors claimed that their MCDHF (GRASP[17–19]) and RCI (FAC[15]) energies "match well", a detailed inspection reveals substantial discrepancies at the high-Z end. For example, for U^{89+}, the two theoretical $2p_{1/2}$ excitation energies differ by 42 eV, deviating from experiment[20] by $+34$ eV and -8 eV, respectively. Similarly, the MCDHF $2p_{3/2}$ result deviates from experiment[21] by 37 eV. These discrepancies contrast sharply with a recent *Nature* study[2] using MDFGME (another GRASP-family code[22]), which achieved sub-eV accuracy for the same level.

Such a difference in accuracy between the mid-Z and high-Z domains questions the reliability of the two relativistic packages in extreme fields. It raises a critical question, particularly for Li-like ions: under what computational conditions can these mainstream frameworks yield consistent and accurate results? From a theoretical standpoint, discrepancies in

†Corresponding author. E-mail: shuangli09@fudan.edu.cn

© 2026 Chinese Physical Society and IOP Publishing Ltd. All rights, including for text and data mining, AI training, and similar technologies, are reserved.

atomic structure calculations generally stem from the Hamiltonian model, the wave function representation, or the numerical implementation. Accordingly, we identify the primary sources of the discrepancies as follows: (i) the completeness of the configuration state function (CSF) basis sets in capturing electron correlation; (ii) the treatment of relativistic interactions, particularly Breit and QED corrections (SE and VP); (iii) the numerical convergence thresholds and grid parameters; and (iv) the subtle, code-specific implementation details that may become significant only in the high-Z regime of the Li-like sequence. Although likely minor, this last factor cannot be ruled out without rigorous investigation. Crucially, the 2007 GRASP2K release,[19] used in the recent study,[16] is a direct precursor to the widely used 2013[23] and 2018[13,14] editions. If such inaccuracies persist in current versions, the reliability of these standard tools for high-Z ions is compromised, necessitating a rigorous re-examination. Here, to resolve these discrepancies, we independently compute the structure of U^{89+} using MCDHF (GRASP2K 2018[13,14]) and RCI (FAC[15]) methods, incorporating electron correlations alongside higher-order relativistic and QED corrections. Due to unspecified computational parameters in Ref. [16], we could not reproduce its results. However, our independent calculations mutually agree and match high-precision experimental data[20,21] within ~ 2 eV, reducing the previously reported gap by an order of magnitude. This confirms that when physical contributions are rigorously treated, both GRASP2K 2018[13,14] and FAC[15] yield consistent, reliable predictions in the strong-field regime. Moreover, the residual ~ 2 eV discrepancy offers an opportunity to develop novel QED model potentials for mainstream atomic packages.

Beyond numerical reconciliation, this work identifies the primary bottlenecks to achieving sub-eV accuracy for each method. For MCDHF, the limiting factor is the precise treatment of SE and VP effects. For RCI, the constraint stems from the local-potential approximation in the initial Dirac–Hartree–Slater orbitals, restricting the subsequent treatment of electron correlation, the Breit interaction, and QED effects. In parallel, we present an extensive U^{89+} dataset to facilitate plasma spectral identification, modeling, and diagnostics.

2. Calculations

To address the pronounced discrepancy reported for high-Z Li-like ions, notably U^{89+},[16] we performed two independent fully relativistic calculations. The first employed the MCDHF method as implemented in the GRASP2K package,[13,14] while the second utilized the RCI approach within the FAC.[15] Both methods systematically targeted the lowest 35 levels of the $1s^2nl$ configurations with $n \leq 6$. Our models incorporate extensive electron correlation and higher-order relativistic effects, including the frequency-independent (Breit0: Gaunt and static retardation) and the additional frequency-dependent (Breitω) corrections. The Breit0 and Breitω constitute the extended Breit interaction, hereafter referred to simply as the Breit interaction.[7] We also accounted for the leading-order QED corrections: SE and VP effects.[8–10] For all considered levels, we determined the excitation energies and generated a complete set of radiative parameters for both allowed (E1) and forbidden transitions, including magnetic dipole (M1), magnetic quadrupole (M2), and electric quadrupole (E2) channels.

2.1. Relativistic configuration interaction

In the RCI (FAC[15]) calculations, the local central potential was optimized with respect to the $1s^22s$ and $1s^22p$ orbitals. In order to ensure a comprehensive treatment of electron correlation and thereby address potential concerns regarding basis-set completeness, we constructed an extensive configuration basis comprising all nl orbitals up to a principal quantum number of $n = 30$. For orbitals with $n \leq 10$, all allowed angular momenta were included, whereas for $11 \leq n \leq 30$, the angular momentum was limited to up to m (i.e., $l \leq 9$). Furthermore, the Hamiltonian incorporated the full Breit interaction (Breit0+Breitω), and the leading-order QED (SE+VP) corrections were taken into account. Finally, the nuclear recoil effect was evaluated and included for completeness, even though it is negligible.

2.2. Multiconfiguration Dirac–Hartree–Fock

As a parallel independent approach, complementary computations were performed using the MCDHF method as implemented in the GRASP2K package.[13,14] The theoretical and computational framework of GRASP2K has been comprehensively outlined in Refs. [14,28,29], and the code has been extensively employed in our recent investigations.[5,30–33] Accordingly, only a brief overview of the computational procedure is provided here.

The multireference (MR) space was defined to comprise all $1s^2nl$ configurations with principal quantum number $n \leq 6$ and orbital angular momentum $l < n$. The $1s^2$ shell was treated as a closed core (C), whereas the outer nl electron was regarded as the valence (V). Consequently, the MR set consisted of eleven even-parity states (2s, 3s, 3d, 4s, 4d, 5s, 5d, 5g, 6s, 6d, and 6g) and nine odd-parity states (2p, 3p, 4p, 4f, 5p, 5f, 6p, 6f, and 6h). The spectroscopic orbitals across these configurations were variationally optimized in a simultaneous manner for all states within the extended optimal level (EOL) scheme,[34] thereby ensuring a balanced and common basis.

Electron correlation was incorporated by systematically enlarging the configuration space through single (S) and double (D) substitutions from *all* electrons in the MR configurations, thereby accounting for both core–valence (CV) and

core–core (CC) interactions. For numerical stability, the treatment of CC correlation was deliberately constrained: double substitutions from the 1s core were restricted to the active set (AS) $\{6s, 6p, 6d, 6f, 6g, 6h\}$. This correlation strategy aided convergence in the subsequent self-consistent-field (SCF) optimization. The correlation space was assembled as a sequence of layered AS orbitals, defined as

$$\begin{aligned} \mathrm{AS0} &= \{6s, 6p, 6d, 6f, 6g, 6h\}, \\ \mathrm{AS1} &= \mathrm{AS0} + \{7s, 7p, 7d, 7f, 7g, 7h, 7i\}, \\ \mathrm{AS2} &= \mathrm{AS1} + \{8s, 8p, 8d, 8f, 8g, 8h, 8i\}. \end{aligned} \tag{1}$$

At each SCF stage, only the newly introduced layer was variationally optimized, while all inner orbitals were held fixed. Convergence of the Dirac–Coulomb energies was closely monitored throughout. Moreover, to control the computational load inherent to the extensive SCF procedures, a selective configuration interaction (CI) approach was employed. Specifically, for each AS, the CI space was restricted to the first-order interaction space, comprising only configuration state functions (CSFs) with a non-zero Hamiltonian coupling to the MR configurations.

Advancing from AS1 to AS2 resulted in a shift of excitation energies below 0.08 eV for all levels considered. Such rapid convergence demonstrates the robustness of the adopted correlation strategy and indicates that residual electron-correlation effects are insignificant within the target precision, thereby excluding basis-set incompleteness as a credible source of the previously reported discrepancies.[16] The final MCDHF atomic parameters were obtained from a large-scale CI calculation based on the optimized AS2 orbital set. At this stage, the configuration space was further expanded to include all single, double, and triple (SDT) substitutions from the MR set into AS2 orbitals. The Hamiltonian, diagonalized over these extensive CSFs, comprised the Dirac–Coulomb operator, the Breit0 and Breitω contributions, along with the leading-order QED (SE+VP) corrections. The nuclear recoil term was omitted owing to its insignificance, consistent with the above RCI results.

Having obtained these final large-scale MCDHF wave functions, we then assessed their reliability by comparing E1 and E2 transition rates computed in the length and velocity gauges (see Table A, which is available in Science Data Bank, with the link https://doi.org/10.57760/sciencedb.32492). For all 334 transitions considered (164 E1 and 170 E2), we evaluated the relative discrepancy dT between the two gauges. Here, dT was defined following Refs. [47,48] as $\mathrm{d}T = \frac{|A_1 - A_2|}{\max(A_1, A_2)}$, where A_1 and A_2 denote the transition rates obtained from the two gauges for a given transition. A smaller dT indicates closer agreement, with d$T = 0$ corresponding to perfect concordance.[6] Overall, the agreement between the gauges was very good: 315 transitions (94%) had d$T < 3\%$. For the E1 transitions, the mean value and standard deviation of dT were 2% and 5%, respectively, whereas the corresponding values for the E2 transitions were 0.5% and 0.9%. Only a small subset of E1 transitions was notably sensitive to the choice of gauge; in particular, for strong transitions involving high principal quantum numbers, such as $2p_{1/2}$–$5s_{1/2}$ and $2p_{1/2}$–$6s_{1/2}$, dT reached about 10%. In the following discussion, unless explicitly stated otherwise, we employ the length gauge. The choice of the length gauge is motivated by its well-established robustness for highly charged ions (HCIs), for which the computed amplitudes have been shown to be largely insensitive to the treatment of negative-energy states in the basis set.[46]

3. Results and discussion

Our large-scale, cross-validated calculations decisively resolve the previously reported puzzling discrepancy of up to ~40 eV in the 2s–2p excitation energies of U^{89+}.[16] For the benchmark $2p_{1/2}$ and $2p_{3/2}$ levels, our MCDHF (GRASP2K version 2018[13,14]) and RCI (FAC[15]) results reduce the theory–experiment gap by an order of magnitude. Crucially, as shown in Table 1, our independent theoretical predictions bracket the high-precision experimental values.[20,21,35,36] The MCDHF energies lie 1.2–1.7 eV below experiment, whilst the RCI values are 0.8–1.8 eV above. This robust bracketing, achieved through two entirely different theoretical frameworks, restores confidence in these general-purpose codes for the high-Z regime and establishes a residual theory–experiment discrepancy of approximately 2 eV. Table 1 also shows that uncertainties (indicated by the error bars) for both high-precision theoretical predictions and experimental measurements are consistently below 0.35 eV, confirming their reliability. Furthermore, Loetzsch *et al.*[2] demonstrated that for the $2p_{3/2}$ level, the cumulative contribution from two-loop and higher-order QED, nuclear recoil and polarization effects remains below 0.2 eV. As this magnitude is significantly smaller than the observed ~ 2 eV deviation, these perturbative factors are ruled out as the primary source of the discrepancy.

To elucidate the origins of both the residual discrepancy and the systematic differences between the two methods, we performed a layer-by-layer decomposition of the physical contributions to the excitation energies. This analysis reveals the bottlenecks intrinsic to each approach in the strong-field regime. At the Dirac–Coulomb level, the MCDHF method demonstrates superior accuracy in its treatment of electron correlation, yielding excitation energies converged to within 0.08 eV, as noted in Subsection 2.2. The superior performance of the MCDHF approach stems from the self-consistent variational optimization of radial orbitals, which constructs a

physically accurate zeroth-order Hamiltonian (H_0). Consequently, the perturbation term (H') is minimized, enabling the efficient capture of residual electron correlation within a compact configuration interaction (CI) space. In contrast, the RCI (FAC[15]) approach exhibits an overestimation of ∼0.3 eV in the Dirac–Coulomb excitation energy. Rooted in the Dirac–Fock–Slater approximation,[15] the RCI method utilizes the local Slater exchange potential[37] that cannot fully account for non-local correlation effects. This results in a suboptimal H_0 and a comparatively larger H', leading to slow convergence and necessitating massive CI expansions to compensate simultaneously for electron correlation and orbital relaxation. However, within the constraints of limited computational resources, even extensive CI expansions still cannot fully rectify the energy bias introduced by the initial orbitals. Therefore, the 0.3 eV discrepancy can be attributed to the suboptimal accuracy of the initial orbitals in the RCI method. Crucially, within the RCI framework, the fidelity of the underlying wavefunctions constitutes a fundamental prerequisite, as only upon such a foundation can reliable Breit and QED corrections (SE+VP) be applied. Potential strategies for improvement include the adoption of more advanced exchange–correlation functionals (e.g., LDA,[38] GGA,[39] Krieger–Li–Iafrate,[40] LC-ωPBE,[41] and OEP[42]) or the importation of higher-fidelity orbitals, such as those generated by GRASP2K[13,14] (C. Y. Chen from Fudan University, private communication), though at the cost of introducing additional procedural complexity by necessitating the coordinated use of two independent computational packages in the atomic-structure workflow.

Table 1. Breit, self–energy (SE), and vacuum–polarization (VP) contributions to the 2p excitation energies (in eV) of U^{89+}.

	$2p_{1/2}$			$2p_{3/2}$		
	MCDHF	RCI	Others	MCDHF	RCI	Others
Dirac–Coulomb	286.15	286.52	···	4514.81	4515.07	···
Breit	36.04	36.60	···	−16.07	−16.33	···
Breit0	36.41	36.95	···	−9.04	−9.41	···
Breitω	−0.37	−0.35	···	−7.03	−6.92	···
Dirac–Coulomb–Breit	322.18	323.12	322.30(Th.)[a], 322.23(Th.)[b]	4498.73	4498.74	4498.75(Th.)[a], 4498.69(Th.)[b]
QED	−42.77	−40.70	−41.54(Th.)[b]	−41.05	−38.54	−39.17(Th.)[b]
SE	−56.07	−53.92	−54.24(Th.)[c]	−56.76	−54.31	···
VP	13.30	13.22	12.56(Th.)[c]	15.71	15.77	···
Total	279.42	282.43	280.59(±0.10)(Exp.)[d], 280.65(±0.02)(Exp.)[e], 280.65(±0.08)(Th.)[b], 280.71(±0.10)(Th.)[f]	4457.68	4460.20	4459.37(±0.35)(Exp.)[g], 4459.55(Exp.)[h], 4459.46(±0.08)(Th.)[b], 4459.57(±0.10)(Th.)[i], 4459.81(±0.17)(Th.)[j]

Note: [a]Theoretical results of Kozhedub *et al.*[43] [b]Theoretical results of Sapirstein and Cheng.[44] [c]Theoretical results of Blundell.[45] [d]Experimental results of Schweppe *et al.*[35] [e]Experimental results of Beiersdorfer *et al.*[20] [f]Theoretical results of Kozhedub *et al.*[51] [g]Experimental results of Beiersdorfer *et al.*[36] [h]Experimental results of Beiersdorfer *et al.*[21] [i]Experimental results of Malyshev *et al.*[52] [j]Theoretical results of Loetzsch *et al.*[2]

This initial inaccuracy in the RCI wavefunctions propagates and is subsequently amplified when higher-order relativistic effects are included. When evaluated using the less accurate RCI wavefunctions, the Breit term[7] introduces an additional level-dependent deviation relative to the MCDHF results. As a consequence, at the Dirac–Coulomb–Breit (DCB) level, the RCI calculation for the $2p_{1/2}$ state overestimates state-of-the-art theoretical benchmarks[43,44] by nearly 1 eV. By contrast, for the $2p_{3/2}$ state, the DCB energies obtained from both methods appear to be in near-perfect agreement. Our layer-by-layer decomposition reveals that the observed agreement stems from a fortuitous cancelation of errors within the RCI calculation, wherein an overestimation of approximately 0.3 eV in the Dirac–Coulomb contribution is nearly exactly compensated by an underestimation of roughly 0.3 eV in the Breit contribution. This finding provides an important cautionary note: apparent agreement when multiple physical effects are considered simultaneously may mask compensating errors in the treatment of specific contributions.

Conversely, this hierarchy of performance is reversed in the treatment of QED (SE+VP) corrections, with the RCI approach achieving notably superior accuracy to the MCDHF method. In particular, the RCI results for the dominant SE contribution (∼ 55 eV) exhibit closer agreement (within 0.8 eV) with rigorous QED calculations[44] than do the corresponding MCDHF values, which underestimate the effect by 1.2–1.9 eV. This clearly identifies the approximate formulation employed for the SE term in the present MCDHF implementation as the principal bottleneck preventing the achievement of sub-eV accuracy. Furthermore, a non-negligible discrepancy of approximately 1 eV is observed in the subdominant QED contribution from VP (∼ 13 eV) in the MCDHF for the $2p_{1/2}$ level when compared with high-precision benchmark calculations.[45] Taken together, these findings underscore that even the subdominant VP contribution requires a rigorous treatment if sub-eV precision is to be achieved.

Table 2. Energies (E, in eV) and lifetimes (τ, in s) of $(1s^2)nl$ levels with $n \leq 6$ for U^{89+}. "Key","Con.", and "j" are the index, configuration, and total angular momentum of a level, respectively. Energies include present MCDHF ($E_{\rm MCDHF}$) and RCI ($E_{\rm RCI}$) ones, along with theoretical results from recent work[16] ($E_{\rm MCDHF0}$ and $E_{\rm RCI0}$ are from their MCDHF and RCI calculations, respectively), Zhang *et al.* ($E_{\rm Zhang}$),[49] Johnson *et al.* ($E_{\rm Johnson}$),[46] and experimental results of Beiersdorfer *et al.* ($E_{\rm Exp.}$).[20,21] Additionally, we have included the lifetimes of these energy levels calculated using the present length-gauge radiative rates (A values) from MCDHF and RCI methods in Table 3, denoted as $\tau_{\rm MCDHF}$ and $\tau_{\rm RCI}$, respectively. $\tau_{\rm Exp.}$ represents the exprimental lifetime of Schweppe *et al.*,[35] and $a \pm b \equiv a \times 10^{\pm b}$.

Key	Con.	j	$E_{\rm MCDHF}$	$E_{\rm RCI}$	$E_{\rm MCDHF0}$	$E_{\rm RCI0}$	$E_{\rm Zhang}$	$E_{\rm Johnson}$	$E_{\rm Exp.}$	$\tau_{\rm MCDHF}$	$\tau_{\rm RCI}$	$\tau_{\rm Exp.}$
1	2s	1/2	0.000	0.000	0.000	0.000	0.00	0.000	0.000	···	···	···
2	2p	1/2	279.419	282.426	314.904	272.549	280.78	281.393	280.645	6.12−11	5.93−11	6.18−11
3	2p	3/2	4457.68	4460.20	4496.14	4458.61	4459.9	4459.95	4459.55	1.17−14	1.17−14	···
4	3s	1/2	18785.8	18788.6	18812.6	18783.5	18802	18788.7	···	1.01−15	1.01−15	···
5	3p	1/2	18858.7	18862.2	18895.6	18853.6	18973	···	···	4.79−16	4.78−16	···
6	3p	3/2	20107.8	20110.7	20145.9	20105.1	20235	···	···	9.13−16	9.06−16	···
7	3d	3/2	20120.7	20123.3	20159.6	20115.6	20255	···	···	2.02−16	2.01−16	···
8	3d	5/2	20438.5	20441.1	20476.6	20432.8	20573	···	···	2.37−16	2.37−16	···
9	4s	1/2	25144.3	25147.0	25178.7	25140.2	25263	···	···	1.57−15	1.55−15	···
10	4p	1/2	25173.2	25176.1	25211.3	25167.8	25299	···	···	8.42−16	8.37−16	···
11	4p	3/2	25694.0	25696.7	25732.4	25689.6	25825	···	···	1.44−15	1.43−15	···
12	4d	3/2	25699.7	25702.1	25737.9	25694.5	25834	···	···	4.60−16	4.57−16	···
13	4d	5/2	25834.9	25837.5	25872.6	25829.5	25969	···	···	5.47−16	5.46−16	···
14	4f	5/2	25835.0	25837.4	25872.6	25829.6	25970	···	···	1.02−15	1.02−15	···
15	4f	7/2	25899.2	25901.5	25937.9	25893.7	26034	···	···	1.07−15	1.07−15	···
16	5s	1/2	28004.1	28006.8	28040.0	27999.4	28131	···	···	2.58−15	2.54−15	···
17	5p	1/2	28018.5	28021.2	28056.3	28013.0	28149	···	···	1.46−15	1.45−15	···
18	5p	3/2	28282.0	28284.5	28320.3	28277.0	28415	···	···	2.38−15	2.35−15	···
19	5d	3/2	28284.9	28287.3	28323.0	28279.6	28419	···	···	8.77−16	8.70−16	···
20	5d	5/2	28354.2	28356.7	28392.4	28348.7	28488	···	···	1.05−15	1.04−15	···
21	5f	5/2	28354.3	28356.7	28392.4	28348.8	28489	···	···	1.93−15	1.93−15	···
22	5g	7/2	28387.3	28389.7	28425.0	28381.8	28522	···	···	3.43−15	3.43−15	···
23	5f	7/2	28387.3	28389.7	28425.0	28381.8	28522	···	···	2.05−15	2.05−15	···
24	5g	9/2	28406.7	28409.1	28445.4	28401.2	28541	···	···	3.51−15	3.51−15	···
25	6s	1/2	29524.8	29527.4	···	···	···	···	···	4.08−15	4.01−15	···
26	6p	1/2	29533.0	29535.5	···	···	···	···	···	2.38−15	2.37−15	···
27	6p	3/2	29683.9	29686.7	···	···	···	···	···	3.75−15	3.71−15	···
28	6d	3/2	29685.7	29688.0	···	···	···	···	···	1.49−15	1.49−15	···
29	6d	5/2	29725.7	29728.1	···	···	···	···	···	1.79−15	1.78−15	···
30	6f	5/2	29725.8	29728.2	···	···	···	···	···	3.27−15	3.27−15	···
31	6g	7/2	29744.9	29747.3	···	···	···	···	···	5.82−15	5.82−15	···
32	6f	7/2	29744.9	29747.3	···	···	···	···	···	3.47−15	3.47−15	···
33	6h	9/2	29756.2	29758.5	···	···	···	···	···	9.01−15	9.01−15	···
34	6g	9/2	29756.2	29758.5	···	···	···	···	···	5.97−15	5.97−15	···
35	6h	11/2	29763.6	29766.0	···	···	···	···	···	9.13−15	9.13−15	···

Finally, the residual ~ 2 eV discrepancy serves as a benchmark for developing next-generation QED model potentials, particularly those incorporating machine-learning techniques.[24–27]

In parallel, we report an extensive dataset for U^{89+}. We have computed the atomic properties of the lowest 35 levels from $1s^2nl$ configurations with $n \leq 6$, by employing two independent fully relativistic approaches: the MCDHF and the RCI methods. For completeness, Table 2 summarizes the excitation energies and level lifetimes for all 35 levels obtained with both approaches, together with relevant theoretical and experimental data from earlier work. Table 3 provides an example of the calculated length-gauge radiative parameters. It should be noted that only a subset of the transition data is presented herein; the complete dataset is available in Science Data Bank, with the link https://doi.org/10.57760/sciencedb.32492. In the table, we list the transition rates (A), absorption oscillator strengths (f), line strengths (S), and the intermethod consistency metric dT.[47,48]

As shown in Fig. 1 and Table 2, the two sets of excitation energies exhibit an almost uniform separation: RCI values lie consistently above the MCDHF predictions by approximately 2.3–3.0 eV for nearly all the levels, except for the $3p_{1/2}$ level, where the difference reaches about 3.5 eV. This discrepancy arises from competing contributions: electron correlation and Breit interactions are treated more effectively in MCDHF, whereas leading-order QED terms (SE+VP) are slightly more precise in RCI calculations, as shown in Table 1. Direct comparison with the most accurate experimental energies for the $2p_{1/2}$ and $2p_{3/2}$ levels[20,21] confirms that both MCDHF and RCI predictions agree with the measurements to within 2 eV, consistent with the above discussions. Further-

more, benchmarking against the many-body perturbation theory (MBPT) results of Johnson *et al.*[46] reveals good agreement for our MCDHF dataset, with deviations of only 2–3 eV. Such robustness contrasts sharply with previous large-scale calculations. For example, the widely used results of Zhang *et al.*,[49] which exclude both Breit and QED effects and treat electron correlation only partially, display systematic discrepancies of 0.4%–0.7% (110–140 eV) relative to our MCDHF values. Similarly, the dataset of recent work[16] exhibits pronounced internal inconsistencies between their own MCDHF (hereafter MCDHF0) and RCI (hereafter RCI0) predictions, thereby limiting applicability in contexts demanding high precision. In particular, the MCDHF0 excitation energies exceed our MCDHF values by 25–40 eV. Given the status of existing data, for the two 2p levels, extremely high precision has already been achieved by existing experimental[21,35] and specialized theoretical studies (e.g., Refs. [2,44,51]), we therefore recommend adopting those values directly. The present work focuses on the high-lying $n = 3$–6 levels, where such data are currently lacking. One of the core values of this study is the order-of-magnitude improvement in accuracy compared with previous large-scale calculations. While excitation energy deviations in the works of Zhang *et al.*[49] and recent work[16] reached ~ 100 eV and tens of eV, respectively, nearly all of our MCDHF and RCI excitation energies for the $n = 3$–6 levels show mutual agreement to within 2.3–3 eV. This accuracy is supported by our results for the two 2p levels, which confirm a precision of ~ 2 eV. Consequently, relative to prior large-scale computations, this work provides highly consistent data for the $n = 3$–6 high-lying levels. We also note that, in Table 2, rounding to six significant figures results in an apparent degeneracy for certain levels (22/23, 31/32, and 33/34). However, these levels remain physically distinct in the raw datasets. For instance, quoting to extended significant figures reveals that the MCDHF excitation energies for the $5g_{7/2}$ and $5f_{7/2}$ levels (22/23) are 28387.279 eV and 28387.328 eV, respectively, whilst the corresponding RCI values are 28389.652 eV and 28389.655 eV.

Table 3. Length–gauge transition properties for U^{89+} obtained from the present MCDHF and RCI calculations (example table). The table lists data for both allowed (E1) and forbidden (M1, E2, and M2) transitions. The indices i and j denote the lower and upper levels, respectively, corresponding to the "Key" in Table 2. The tabulated quantities are the transition wavelength λ (in Å), the radiative rate A (in s^{-1}), the dimensionless absorption oscillator strength f, and the line strength S (in a.u., 1 a.u. $= 6.460 \times 10^{-36}$ $cm^2 \cdot esu^2$). The quantity dT represents the relative deviation between the two sets of A values,[47,48] and $a \pm b \equiv a \times 10^{\pm b}$. Note: only a representative subset of the data is listed here, the complete dataset is available in Science Data Bank, with the link https://doi.org/10.57760/sciencedb.32492.

i	j	Type	λ_{MCDHF}	λ_{RCI}	A_{MCDHF}	f_{MCDHF}	S_{MCDHF}	A_{RCI}	f_{RCI}	S_{RCI}	dT
1	2	E1	4.4372+01	4.3900+01	1.635+10	4.826−03	1.410−03	1.686+10	4.872−03	1.408−03	3.1−02
1	3	E1	2.7814+00	2.7798+00	8.494+13	1.970−01	3.608−03	8.504+13	1.970−01	3.606−03	1.2−03
1	3	M2	2.7814+00	2.7798+00	1.178+09	2.732−06	5.260−02	1.180+09	2.733−06	5.253−02	1.5−03
1	5	E1	6.5744−01	6.5731−01	2.074+15	1.344−01	5.817−04	2.080+15	1.348−01	5.832−04	3.1−03
1	6	E1	6.1660−01	6.1651−01	1.073+15	1.224−01	4.967−04	1.076+15	1.227−01	4.979−04	2.8−03
1	6	M2	6.1660−01	6.1651−01	3.211+11	3.660−05	7.677−03	3.222+11	3.672−05	7.698−03	3.5−03
1	7	M1	6.1620−01	6.1612−01	8.740+09	9.950−07	3.032−04	8.772+09	9.984−07	3.042−04	3.7−03
1	7	E2	6.1620−01	6.1612−01	4.912+13	5.593−03	1.559−05	4.916+13	5.595−03	1.559−05	6.9−04
1	8	E2	6.0662−01	6.0654−01	5.105+13	8.449−03	2.247−05	5.109+13	8.453−03	2.247−05	7.1−04
⋮	⋮	⋮	⋮	⋮	⋮	⋮	⋮	⋮	⋮	⋮	⋮

Taken together, these consistent energies provide a reliable foundation for the subsequent analysis of radiative properties. In particular, the computed transition rates for both allowed (E1) and forbidden (M1, E2, M2) channels reveal exceptional concordance between our MCDHF and RCI datasets. As shown in Table 3, the relative deviations are minimal: for the majority of (over 85%) strong ($A > 10^7$ s^{-1}) E1 transitions, the agreement is better than 1%, as illustrated in Fig. 2; similarly, for strong forbidden channels, more than 90% of the strong M1, E2, and M2 rates match within 2%. We note that, in Table 3 (complete table), owing to rounding to five significant figures, the MCDHF and RCI wavelengths for certain transitions (e.g., 2–6 and 2–11) appear numerically identical. However, inspection at higher numerical resolution reveals that the values remain distinguishable. For the 2–6 transition, for instance, the MCDHF and RCI wavelengths are actually 6.25287×10^{-1} Å and 6.25291×10^{-1} Å, respectively. Such good agreement sharply contrasts with the widely used dataset of Zhang *et al.*,[49] where deviations from our MCDHF ones frequently (8 out of 23 transitions) exceed 5% and even reach up to 8%, stemming directly from their incomplete physical model. We note that the four MBPT transitions reported by Johnson *et al.*[46] agree with our MCDHF rates within 2%, except for the $2p_{1/2}$–$3s_{1/2}$ transition, whose value is 6% higher in their work, whereas for this transition our two datasets agree to within 1.5%. Likewise, the two MCDHF transitions from Cheng *et al.*[50] are consistent with our MCDHF results within 3%. Although recent work[16] also provided E1 transition rates, the substantial discrepancies in their computed energies render meaningful comparison infeasible.

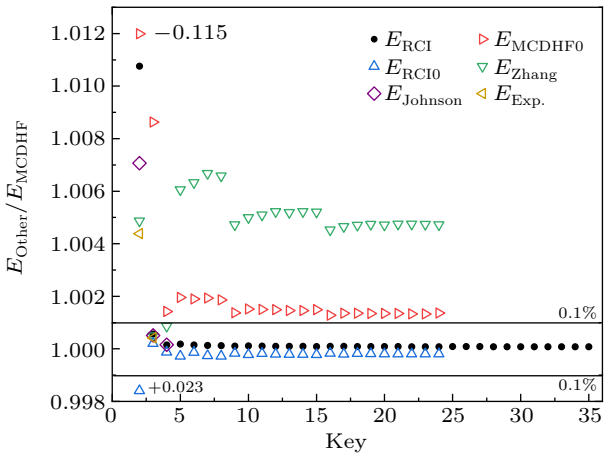


Fig. 1. Comparison of energies with those from the present MCDHF calculations ($E_{\rm MCDHF}$) for the $(1s^2)$ nl levels with $n \leq 6$ for U^{89+}. The other energies include present RCI ones ($E_{\rm RCI}$), along with theoretical results from recent work[16] ($E_{\rm MCDHF0}$ and $E_{\rm RCI0}$ are from their MCDHF and RCI calculations, respectively), Zhang *et al.* ($E_{\rm Zhang}$),[49] Johnson *et al.* ($E_{\rm Johnson}$),[46] and experimental results of Beiersdorfer *et al.* ($E_{\rm Exp.}$).[20,21] The horizontal coordinate"Key" is defined in Table 2. For clarity, we adjust the original energy ratios for Key = 2 (i.e., $2p_{1/2}$) from MCDHF0[16] by subtracting 0.115 and for Key = 3 (i.e., $2p_{3/2}$) from RCI0[16] by adding 0.023. The two horizontal lines indicate relative differences of 0.1%.

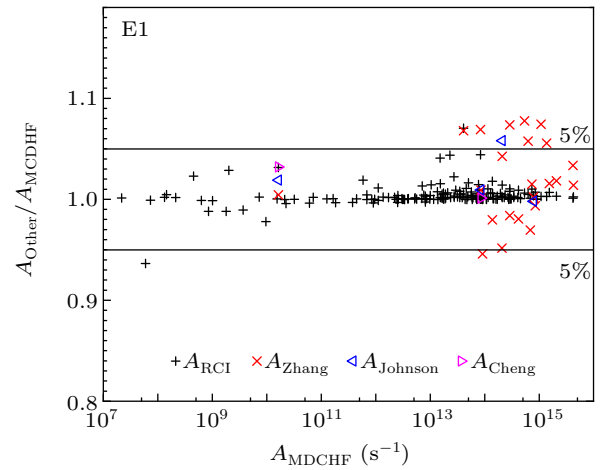


Fig. 2. Comparisons of other theoretical A values with the present MCDHF length-gauge ones ($A_{\rm MCDHF}$) of strong E1 transition. Here, other theoretical A values are from the present RCI length-gauge ones ($A_{\rm RCI}$), as well as from calculations by Zhang *et al.* ($A_{\rm Zhang}$),[49] Johnson *et al.* ($A_{\rm Johnson}$),[46] and Cheng *et al.* ($A_{\rm Cheng}$),[50] respectively. The data between the two horizontal lines indicate that the agreement is within 5%.

This high degree of intermethod agreement translates directly into reliable lifetime predictions. Lifetimes are evaluated according to Ref. [5]: $\tau_j = 1/\sum_i A_{ij}$, where i denotes all lower levels accessible via radiative decay from j. For radiative rates, we include all E1, M1, E2, and M2 channels. Our MCDHF and RCI lifetimes agree to within 2% for 33 of the 34 excited levels, and all values are within 3%. Crucially, for the measured $2p_{1/2}$ lifetime,[35] our MCDHF (6.12×10^{-11} s) and RCI (5.93×10^{-11} s) values are lower than experiment (6.18×10^{-11} s) by only 1% and 4%, respectively. This close agreement provides definitive experimental validation of the present study. Nevertheless, further high-precision experimental measurements are urgently needed to permit more rigorous and extensive benchmarking of the present calculations.

4. Conclusion

In summary, we have resolved a challenging theoretical inconsistency in the excitation energies of U^{89+} through a systematic investigation. Our analysis demonstrates that, when a sufficiently comprehensive treatment of all significant physical contributions is applied, both MCDHF and RCI methods can yield mutually consistent results, thereby reducing the theory–experiment discrepancy to approximately 2 eV. We have identified the principal bottlenecks to achieving sub-eV precision: in MCDHF, accuracy is primarily limited by QED corrections, particularly the SE term. Furthermore, achieving sub-eV precision still requires rigorous treatment of the VP term. By contrast, in the RCI approach, improving the low-accuracy wavefunctions derived from a Slater local central potential is a prerequisite. Beyond addressing the ~ 40 eV discrepancy, this study represents a significant advance in the frontier of general-purpose atomic packages for high-Z systems. Importantly, the remaining ~ 2 eV gap should be regarded as a well-quantified challenge, thereby opening a promising avenue for investigations extending beyond current QED model potentials. Furthermore, we present a comprehensive dataset encompassing excitation energies for the lowest 35 levels with $n \leq 6$, radiative properties for both allowed (E1) and forbidden (M1, E2, M2) transitions, together with the corresponding lifetimes. The results from the two methods exhibit excellent mutual agreement and align closely with high-precision experimental and theoretical benchmarks: our estimates indicate excitation energies accurate to within ~ 2 eV, while theoretical uncertainties for most strong allowed (E1) and forbidden (M1, E2, M2) transitions remain below 1% and 2%, respectively. To the best of our knowledge, this constitutes the most extensive cross-validated dataset for this ion to date, providing valuable applications in plasma spectroscopy.

Data availability statement

The data that support the findings of this study are openly available in Science Data Bank at the following link https://doi.org/10.57760/sciencedb.32492.

Acknowledgments

Project supported by the Research Foundation for Higher Level Talents of West Anhui University (Grant No. WGKQ2021005) and the Research Projects of West Anhui University (Grant No. WXZR202418).

The author (S. L.) acknowledges the support from the Visiting Researcher Programs at Fudan University (C. Y. Chen's

research group) and the Institute of Applied Physics and Computational Mathematics (J. Yan's research group). The author (S. L.) would also like to express his gratitude to Ai-Jia Wang, Chen-Jie Xi, Xiang Gao, and Ying-Hong Shi for many valuable discussions during this research.

References

[1] Barnes J, Zhu Y L, Lund K A, Sprouse T M, Vassh N, McLaughlin G C, Mumpower M R and Surman R 2021 *Astrophys. J.* **918** 44
[2] Loetzsch R, Beyer H F, Duval L, *et al.* 2024 *Nature* **625** 673
[3] Smits O R, Indelicato P, Nazarewicz W, Piibeleht M and Schwerdtfeger P 2023 *Phys. Rep.* **1035** 1
[4] King S A, Spiess L J and Micke P, *et al.* 2022 *Nature* **611** 43
[5] Li S, Zhao M, Liu G Q, Hu C B and Pan G Z 2023 *Chin. Phys. B* **32** 103101
[6] Li S, Zhou J, Zhu L H, Mei X F and Yan J 2024 *Chin. Phys. B* **33** 103102
[7] Rodrigues G C, Ourdane M A, Bieroń J, Indelicato P and Lindroth E 2000 *Phys. Rev. A* **63** 012510
[8] Shabaev V M, Tupitsyn I I, Kaygorodov M Y, Kozhedub Y S, Malyshev A V and Mironova D V 2020 *Phys. Rev. A* **101** 052502
[9] Li M C, Si R, Brage T, Hutton R and Zou Y M 2018 *Phys. Rev. A* **98** 020502
[10] Si R, Guo X L, Brage T, Chen C Y, Hutton R and Fischer C F 2018 *Phys. Rev. A* **98** 012504
[11] Li S 2024 arXiv:2412.10613 [physics.atom-ph]
[12] Yerokhin V A and Surzhykov A 2018 *J. Phys. Chem. Ref. Data* **47** 023105
[13] Fischer C F, Gaigalas G, Jönsson P and Bieroń J 2019 *Comput. Phys. Commun.* **237** 184
[14] Jönsson P, Gaigalas G, Fischer C F, *et al.* 2023 *Atoms* **11** 68
[15] Gu M F 2008 *Can. J. Phys.* **86** 675
[16] Kumar P, Goyal A and Mohan M 2022 *Eur. Phys. J. Plus* **137** 1253
[17] Grant I P, McKenzie B J, Norrington P H, Mayers D F and Pyper N C 1980 *Comput. Phys. Commun.* **21** 207
[18] Parpia F A, Fischer C F and Grant I P 1996 *Comput. Phys. Commun.* **94** 249
[19] Jönsson P, He X, Fischer C F and Grant I P 2007 *Comput. Phys. Commun.* **177** 597
[20] Beiersdorfer P, Chen H, Thorn D B and Träbert E 2005 *Phys. Rev. Lett.* **95** 233003
[21] Beiersdorfer P, Elliott S R, Osterheld A, Stöhlker T, Autrey J, Brown G V, Smith A J and Widmann K 1996 *Phys. Rev. A* **53** 4000
[22] Desclaux J P 1975 *Comput. Phys. Commun.* **9** 31
[23] Jönsson P, Gaigalas G, Bieroń J, Fischer C F and Grant I P 2013 *Comput. Phys. Commun.* **184** 2197
[24] Bilous P, Cheung C and Safronova M 2024 *Phys. Rev. A* **110** 042818
[25] Bilous P, Palffy A and Marquardt F 2023 *Phys. Rev. Lett.* **131** 133002
[26] Ma K C, Yang C, Zhang J Y, Li Y F, Jiang G and Chai J J 2024 *Entropy* **26** 962
[27] Chen Z B 2024 *J. Quant. Spectrosc. Radiat. Transf.* **324** 109078
[28] Fischer C F, Godefroid M, Brage T, Jönsson P and Gaigalas G 2016 *J. Phys. B: At. Mol. Opt. Phys.* **49** 182004
[29] Jönsson P, Godefroid M, Gaigalas G, *et al.* 2022 *Atoms* **11** 7
[30] Wang K, Si R, Dang W, *et al.* 2016 *Astrophys. J. Suppl. Ser.* **223** 3
[31] Wang K, Jönsson P, Ekman J, Gaigalas G, Godefroid M R, Si R, Chen Z B, Li S, Chen C Y and Yan J 2017 *Astrophys. J. Suppl. Ser.* **229** 37
[32] Si R, Li S, Guo X L, Chen Z B, Brage T, Jönsson P, Wang K, Yan J, Chen C Y and Zou Y M 2016 *Astrophys. J. Suppl. Ser.* **227** 16
[33] Wang K, Chen Z B, Si R, *et al.* 2016 *Astrophys. J. Suppl. Ser.* **226** 14
[34] Dyall K G 1986 *Aust. J. Phys.* **39** 667
[35] Schweppe J, Belkacem A, Blumenfeld L, *et al.* 1991 *Phys. Rev. Lett.* **66** 1434
[36] Beiersdorfer P, Knapp D, Marrs R E, Elliott S R and Chen M H 1993 *Phys. Rev. Lett.* **71** 3939
[37] Slater J C 1951 *Phys. Rev.* **81** 385
[38] Kohn W and Sham L J 1965 *Phys. Rev.* **140** A1133
[39] Perdew J P, Burke K and Ernzerhof M 1996 *Phys. Rev. Lett.* **77** 3865
[40] Krieger J B, Li Y and Iafrate G J 1992 *Phys. Rev. A* **46** 5453
[41] Vydrov O A and Scuseria G E 2006 *J. Chem. Phys.* **125** 234109
[42] Talman J D and Shadwick W F 1976 *Phys. Rev. A* **14** 36
[43] Kozhedub Y S, Volotka A V, Artemyev A N, Glazov D A, Plunien G, Shabaev V M, Tupitsyn I I and Stöhlker T 2010 *Phys. Rev. A* **81** 042513
[44] Sapirstein J and Cheng K T 2011 *Phys. Rev. A* **83** 012504
[45] Blundell S A 1993 *Phys. Rev. A* **47** 1790
[46] Johnson W R, Liu Z W and Sapirstein J 1996 *At. Data Nucl. Data Tables* **64** 279
[47] Fischer C F 2009 *Phys. Scr.* **T134** 014019
[48] Ekman J, Godefroid M R and Hartman H 2014 *Atoms* **2** 215
[49] Zhang H L, Sampson D H and Fontes C J 1990 *At. Data Nucl. Data Tables* **44** 31
[50] Cheng K T, Kim Y K and Desclaux J P 1979 *At. Data Nucl. Data Tables* **24** 111
[51] Kozhedub Y S, Andreev O V, Shabaev V M, Tupitsyn I I, Brandau C, Kozhuharov C, Plunien G and Stöhlker T 2008 *Phys. Rev. A* **77** 032501
[52] Malyshev A V, Kozhedub Y S and Shabaev V M 2023 *Phys. Rev. A* **107** 042806